Edge Detection on Interval-Valued Images

Chapter · September 2011

DOI: 10.1007/978-3-642-24001-0_30

C. Lopez-Molina
Universidad Pública de Navarra

Bernard De Baets
Ghent University

Edurne Barrenechea
Universidad Pública de Navarra

Humberto Bustince Sola
Universidad Pública de Navarra

Edge detection on interval-valued images

C. Lopez-Molina, B. De Baets, E. Barrenechea, H. Bustince

Abstract A digital image is an approximation of some real situation, and carries some uncertainty. In this work we model the ambiguity related to the brightness by associating an interval with each pixel, instead of a scalar brightness value. Then we adapt the Sobel method for edge detection to the new conditions of the image, leading to a representation of the edges in the shape of an interval-valued fuzzy set. To conclude, we illustrate the performance of the method and perform a qualitative comparison with the classical Sobel method on grayscale images.

1 Introduction

Any discretization process is based on sampling continuous facts, and hence misses part of the initial information. Moreover, the data can be contaminated in many different ways. In the case of a digital image, different factors are to be taken into account, either inherent to the model (as the limited number of tones) or alien to it (as noise or broken cells in the sensor). Hence, we can never have a full certainty about the tone of a pixel. In the field of edge detection, the problems originating from this uncertainty manifest themselves clearly, since sometimes not even two humans can reach an agreement on where the boundary between two objects is.

Fuzzy logic has been used in many different fields. Applications have been published, especially in those tasks where factors as ambiguity and partial or contradictory information arise. When considering classical fuzzy sets (FS), the membership of each element to a set is expressed by a degree in $[0,1]$. Subsequently, many ex-

C. Lopez-Molina, E. Barrenechea and H. Bustince
Dpto. Automatica y Computacion, Universidad Publica de Navarra, Spain; e-mail: carlos.lopez@unavarra.es

B. De Baets
Department of Applied Mathematics, Biometrics and Process Control, Ghent University, Belgium; e-mail: bernard.debaets@ugent.be

tensions have been proposed in order to model the fuzziness, giving rise to different *extensions* or *generalizations* of the fuzzy sets. Among these extensions, one of the most popular ones has been the interval-valued fuzzy sets (IVFS), which represent membership by means of an interval $[a,b]$, $a,b \in [0,1]$.

Due to the nature of digital images, fuzzy logic appears as a natural option for handling the uncertainty. In fact, in the image processing field, edge detection has been one of the tasks where fuzzy logic has been most prolific. It has been used for different purposes at almost any step of the process, from the very interpretation of the image [1, 2] to the reconstruction of the edges once they have been characterized [3]. Authors have experimented with a wide variety of techniques based on fuzzy logic, including fuzzy inference systems [4, 5], fuzzy morphology [6], and fuzzy peer groups [7]. However, most of the applications make use of FS, partly because of the relatively new development of the FS extensions.

In this work we introduce and justify an interval-based representation of images, designed for better managing their inherent ambiguity. Then, we present the extension of the classical Sobel method [8] for its application on interval-valued images, leading to a representation of the edges based on IVFS. We also show how to turn the IVFS representation of the edges into a binary edge image.

The remainder of this work is organized as follows. Section 2 is devoted to the analysis and modeling of the ambiguity in digital images. Section 3 introduces the extension of the Sobel method for edge detection to interval-valued images. To conclude, we include experimental tests in Section 4 and draw some brief conclusions in Section 5.

2 Images and ambiguity representation

2.1 Image representation

In this work we consider an image to be a matrix of M rows and N columns, with $P = \{1,\ldots,M\} \times \{1,\ldots,N\}$ the set of their positions. In an image I, the value of a pixel at a position $(x,y) \in P$, $I_{(x,y)}$ is a value in $\{0,\ldots,255\}$. Moreover, we denote as $n(x,y) \subset P$ to the set of positions in a 3×3 neighborhood centered at (x,y).

2.2 Images and inherent ambiguity

Digital images are the result of a discretization of the reality. That is, a discrete, sampled version of a continuous fact. Hence, there are different sources of uncertainty and ambiguity to be considered when performing image processing tasks. Most of those sources are contextual, in the sense that they could be present (or not) in an image, depending on the situation the image was registered at. Some examples of those sources of contamination are noise, excessive illumination or shading. However, there is also some uncertainty embedded in the very nature of digital images: the measurement error. The image discretizes the reality in two different facets, spatial and tonal, each of them producing a measurement error:

- *Spatial error:* Surfaces and objects are continuous in reality. However, they become discrete in the pixel representation of an image. Hence, due to the way the information is stored, we might be mislocating one object by 1 position in any direction.
- *Tonal error:* Images are stored using a finite number of tones. There are usually 2^8 tones in a greyscale image, or 2^{24} in a RGB one. However, even using finer-detail coding, there is always a limit in the tonal precision. Hence, the measure error associated to the tone of the pixel is as much as ± 1 tone.

In fact, both errors are derived from the imprecision of the discrete measure used in each dimension (spatial and tonal). A scalar representation of the pixel brightness is not sufficient for representing both errors. Hence, we will use an interval-valued representation of the image brightness. The construction will be straight, driven from the analysis of the measurement errors performed above. From an image I, we will generate an interval-valued (IV) image W so that the value at each pixel (x,y) is obtained as

$$W_{(x,y)} = \left[\max(0, \min_{(x',y')\in n(x,y)} I_{(x',y')} - 1),\ \min(255, \max_{(x',y')\in n(x,y)} I_{(x',y')} + 1)\right]. \quad (1)$$

That is, we assign to each position in the image an interval encompassing all of the brightness values in a 3×3 neighborhood (assuming the spatial error), modified by ± 1 tone (because of the tonal error). Fig. 1 includes as an example the Lena image, togheter with the upper and lower bound of its interval-valued representation.

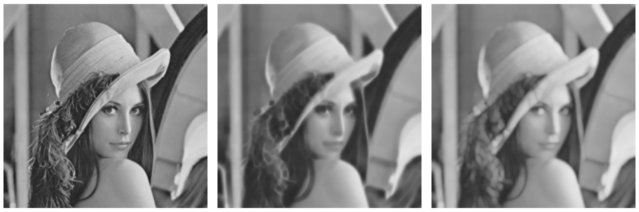

(a) Original Image (b) IV representation

Fig. 1 The Lena image and the lower and upper bounds of its interval valued representation.

We have to bear in mind that the construction of IV images is quite robust against some specific types of noise (as Gaussian one), but also quite sensitive to some other kinds of contamination (as salt-and-pepper). However, dealing with external sources of contamination is not the main goal of the methodology, since we only intend to capture those factors intrinsically linked to the image representation.

The IV images provide a realistic interpretation of the image, since the measurement error is something we should not ignore. However, there are very few procedures in the image processing field able to deal with such a representation of the images [9]. We devote the rest of this paper to generalize the Sobel method for edge detection on IV images.

3 The Sobel method and its application on interval-valued images

3.1 The Sobel method

The Sobel method for edge detection is based on filtering an image with 2 operators, each of them in charge of estimating the intensity change along one of the axis (horizontal and vertical). The estimation of the change along each axis is later used for generating the so-called *gradients*. Gradients are vectors representing the strength and direction of the intensity changes at each position of the image.

Horizontal Operator

-1		1
-2		2
-1		1

Vertical Operator

1	2	1
-1	-2	-1

Fig. 2 The Sobel operators for edge detection.

The Sobel operators (included in Fig. 2) act as discrete convolution operators, producing an approximation of each of the components of the gradient at each point. Some considerations on the search for gradients in discrete environments can be found in [10, 11]. For example, the normalized estimation of the horizontal intensity change at a position of the image ($H_{(x,y)} \in [-1,1]$), is obtained as

$$H_{(x,y)} = \frac{1}{4 \cdot 255} \sum \begin{pmatrix} -1 & 0 & 1 \\ -2 & 0 & 2 \\ -1 & 0 & 1 \end{pmatrix} * \begin{pmatrix} I_{(x-1,y+1)} & I_{(x,y+1)} & I_{(x+1,y+1)} \\ I_{(x-1,y)} & I_{(x,y)} & I_{(x+1,y)} \\ I_{(x-1,y-1)} & I_{(x,y-1)} & I_{(x+1,y-1)} \end{pmatrix}, \qquad (2)$$

where $*$ represents the convolution operator. The vertical estimation ($V_{(x,y)}$) is calculated analogously.

Then, the gradient at a given position (x,y) is constructed as $\mathbf{G}_{(x,y)} = (H_{(x,y)}, V_{(x,y)})$. Once the information is taken as a gradient, many different techniques become applicable for turning the edges into a binary representation. Fig. 3 includes an example of the application of the Sobel method on the Lena image. The gradient magnitudes have been used to generate an intermediate representation of the edges, in the shape of a FS. In order to do so, we have selected the normalized Euclidean norm $||\mathbf{G}_{(x,y)}|| = \frac{1}{\sqrt{2}}\sqrt{H^2_{(x,y)} + V^2_{(x,y)}}$. (See [12] for further considerations on other options for combining the gradient components). To conclude, the conversion into binary edges has been carried out using the non-maximum suppression (NMS) [13] and the Rosin method for thresholding [14].

The Sobel method [8], as well as the Prewitt method [15], has had great impact in the literature. They are considered the pioneer methods in the derivative-based approach to edge detection [11, 16, 17], that has provided some of the most recognized methods in the literature, such as the Canny [13] or Marr-Hildreth [18] methods.

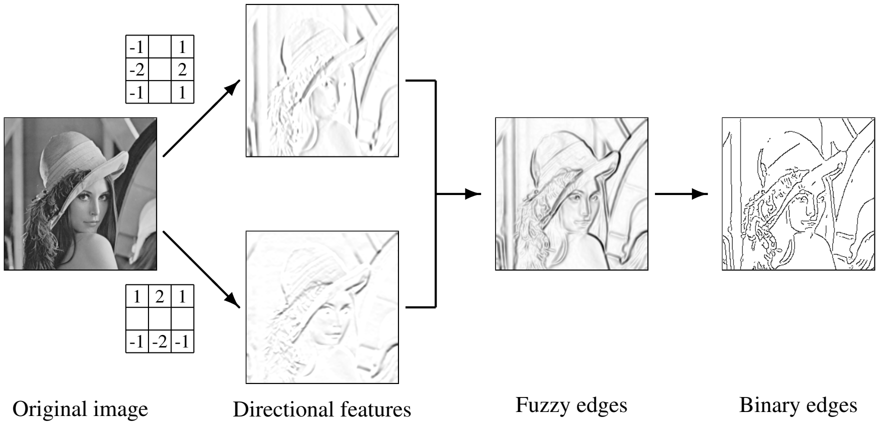

Fig. 3 Schematic representation of the Sobel edge detection method

3.2 *Application to interval-valued images*

Once we have IV images, there are different options to apply the Sobel operators. For example, we could think of applying the detector individually on the upper and lower bounds of the intervals, as they are be themselves scalar images. However, this collides with the main idea behind the IV representation of the images. Hence, we will apply the classical interval operations [19]:

- Sum of intervals: $[\underline{a},\overline{a}] + [\underline{b},\overline{b}] = [\underline{a}+\underline{b},\overline{a}+\overline{b}]$;
- Difference of intervals: $[\underline{a},\overline{a}] - [\underline{b},\overline{b}] = [\underline{a}-\overline{b},\overline{a}-\underline{b}]$;
- Product of a positive scalar s and an interval: $s \cdot [\underline{a},\overline{a}] = [s \cdot \underline{a}, s \cdot \overline{a}]$

In this way, both the horizontal and vertical intensity changes are expressed as intervals. More specifically, they are subintervals of $[-1,1]$. As a consequence, the gradient estimated at the position p will no longer be a vector in the $[-1,1]^2$ space, but an area, as illustrated in Fig. 4(a). This area can be seen as a projection of the uncertainty about the intensity of the pixels in the image (and the object boundaries). We are unsure about the initial data, so the uncertainty is propagated when measuring local features (in this case, the gradient). Following this interpretation of the image brightness, we understand that the gradient is located somewhere in the gray area in Fig. 4(a), while its exact position remains unknown.

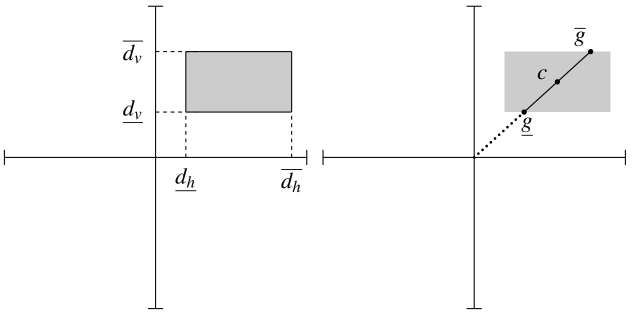

(a) Area-based interpretation (b) Interval-valued gradient

Fig. 4 Area gradient

The area-based interpretation has a complicated application. Moreover, our goal to obtain of binary edges, following the constraints by Canny [13]. The first step in binarization of the edges is the conversion of the area into a segment. There are different ways of performing the geometric interpretation of the area in Fig. 4(a). We propose to first calculate the center of gravity of the area,

$$c = \left[\frac{\underline{d_h} + \overline{d_h}}{2}, \frac{\underline{d_v} + \overline{d_v}}{2} \right] \tag{3}$$

Then, the candidates for being the gradient are those points in the intersection of the area and the straight line passing through the origin c. Note that, in case c coincides with the origin, we have a null gradient. This segment is delineated by $\underline{g}$ (the closest point to the origin) and $\overline{g}$ (the one furthest away), as illustrated in Fig. 4(b).

In order to follow the Sobel method as closely as possible, we have to generate a FS representing the edges. However, in our case, instead of creating directly a classical FS, we will first use an IVFS. The interval-valued membership degree will be determined by $[||\underline{g}||, ||\overline{g}||]$, where d stands for the normalized Euclidean norm, as before. Before using the classical procedures for binarization, the IVFS representation of the edges will be turned into a FS. To do so we will use the K_α operators, defined as $K_\alpha([\underline{a},\overline{a}]) = (\underline{a} + \alpha(\overline{a} - \underline{a}))$. In this way, $\alpha \in [0,1]$ will measure our optimism with respect to the magnitude of the gradients. Once the edges are modeled in the shape of a FS, the processing is as it was in Fig. 3. We will first use NMS for thinning the edges, then the Rosin method for binarization. In this way we obtain an edges representation satisfying the Canny constraints [13].

This method for edge detection, as illustrated in Fig. 5, will be called the Interval-valued Sobel (IV-Sobel) method.

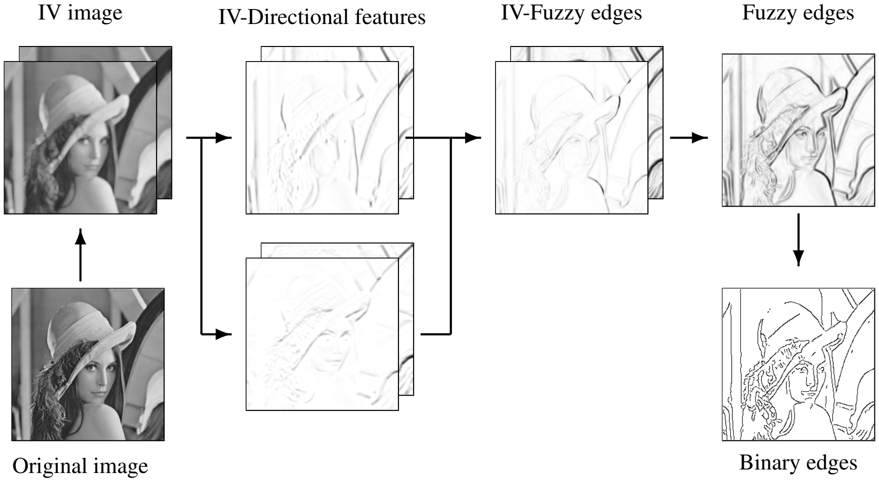

Fig. 5 Visual schema of the IV-Sobel edge detection method

In order to illustrate the performance of the proposed method, we use the Lena image in Fig. 1(a). First, we have regularized the image with a Gaussian filter with $\sigma = 1.80$. At the moment of creating a FS representation of the edges we have experimented with different values of α. The results are included in Fig. 6. Note that the upper and lower bounds of the IVFS are the FSs generated with $\alpha = 0.0$ and $\alpha = 1.0$, respectively. In this figure we observe how the increase of the optimism (represented by an increase of α) gives rise to the selection of a larger number of edge points. However, it remains unclear whether that is bad or good news, since it has both positive and negative consequences. For example, in Fig. 6 we can observe how the hat silhouette is almost completed using large values of α, but they also imply a lot of false positive detections, as those in the hair region.

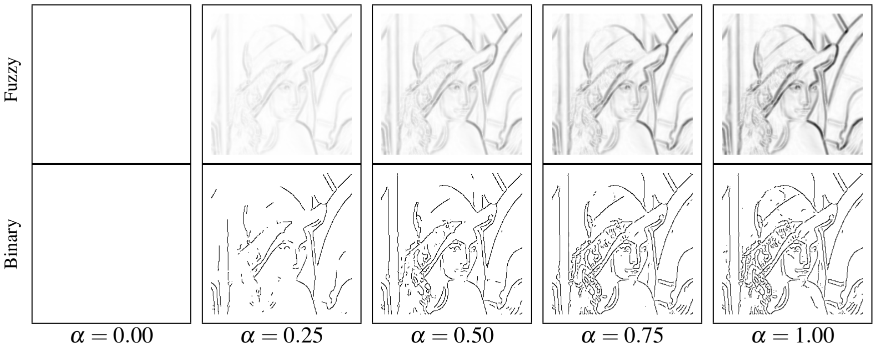

Fig. 6 Fuzzy and binary edge images obtained using different α values for the conversion of the IVFSs into FSs.

4 Experimental results

4.1 Aim of the experiment

In this experiment we want to compare the performance of the classical Sobel method with that of the IV-Sobel method. In order to do so, we have run both of the algorithms on the same images, under similar conditions, and then quantified the results.

4.2 Experimental dataset

In the experiments we have used the Berkeley Segmentation Dataset (BSDS) [20], containing 300 images. The images are provided in grayscale with 256 tones and have a resolution of 481 × 321 (or 321 × 481) pixels. In addition, each of them comes along with 5 to 10 hand-made segmentation solutions. As those solutions are provided in the shape of region boundaries, we have used them as ground truth for the quantification of the quality of the edge detection results.

4.3 Comparison method

Baddeley's Delta Metric (BDM) is a measure initially designed for the comparison of binary sets [21], but can also be used to compare binary images. It intends to measure the similarity of two subsets of *featured* points on the same referential. As the edges of an image are usually displayed as a binary image (following the Canny constraints [13]), this measure can be used for our purposes.

Let B_1 and B_2 be two binary images and let M,N and P be as defined in Section 2. Given a value $1 < k < \infty$ the k-BDM between the images B_1 and B_2 (denoted $\Delta^k(B_1,B_2)$) is defined as:

$$\Delta^k(B_1,B_2) = \left[\frac{1}{|P|} \sum_{p \in P} |w(d(p,B_1)) - w(d(p,B_2))|^k \right]^{\frac{1}{k}} , \tag{4}$$

where $d(p,B_i)$ represents a distance from the position p to the closest *featured* point of the image B_i and $w : [0,\infty] \to [0,\infty]$ is a concave, increasing function used for weighing. Note that we assume that both images contain at one or more edge pixels. In our experiments, we use the Euclidean distance in the computation of d. Hence, $d(p,B_i)$ stands for the minimum Euclidean distance from the position p to an edge point of B_i. As for the other settings, we use $w(x) = x$ [22, 23]. and $k = 2$, as in [23].

The score of an edge detection method on an image is the average distance of its result to the set of hand-made solutions associated with that image. Analogously, the score on a dataset is the average on its images.

4.4 Algorithm

Algorithm 1 lists all of the steps of the procedure. The proposed algorithm could be modified in order to obtain better results. For example, single-threshold binarization techniques are usually outperformed by double-threshold techniques (as *hysteresis*), specially on low contrast regions. Also the Gaussian smoothing could be substituted by edge preserving techniques [24]. However, the aim of this experiment is not to obtain the best possible results, but to perform a comparison between the Sobel and the IV-Sobel methods.

```
Data: An image $I$, an optimism indicator $\alpha$
Result: A binary edge image $B$
begin
    Smoothen $I$ with a Gaussian mask with standard deviation $\sigma_1 = 1.0$;
    Create the IV version of the image, $I_w$;
    Calculate the IV gradient estimations $H_w$ and $V_w$;
    Using the technique in Fig. 4, generate the IV fuzzy edges $E_w$;
    Create the fuzzy edges as $E = K_\alpha(E_w)$;
    Obtain a thin version of fuzzy edge image ($T$) using NMS [13];
    Obtain a binary edge image $B$ from $T$ using Rosin method [14];
end
```

Algorithm 1: Algorithm of the IV-Sobel method with user-selected value α.

4.5 Results

We have executed the algorithm on the 100 images of the BSDS *test* set [20], using different fixed $\alpha \in \{0, 0.025, \dots, 1\}$. Fig. 7 displays the average performance on the image set, and its comparison with the performance obtained by the classical Sobel method. In addition, we display the average number of pixels classified as edges for each value of α ($|B_\alpha|$) and its increase.

We observe how the results by the Sobel method can be greatly improved by the IV-Sobel one. First, there is an initial range of values of α producing very bad results, but then the performance rapidly increases. Then, when α tends to 1, the performance of the Sobel and IV-Sobel methods becomes similar. Moreover, we notice that the best results (average BDM) coincide with those values of α producing largest increments of $|B_\alpha|$.

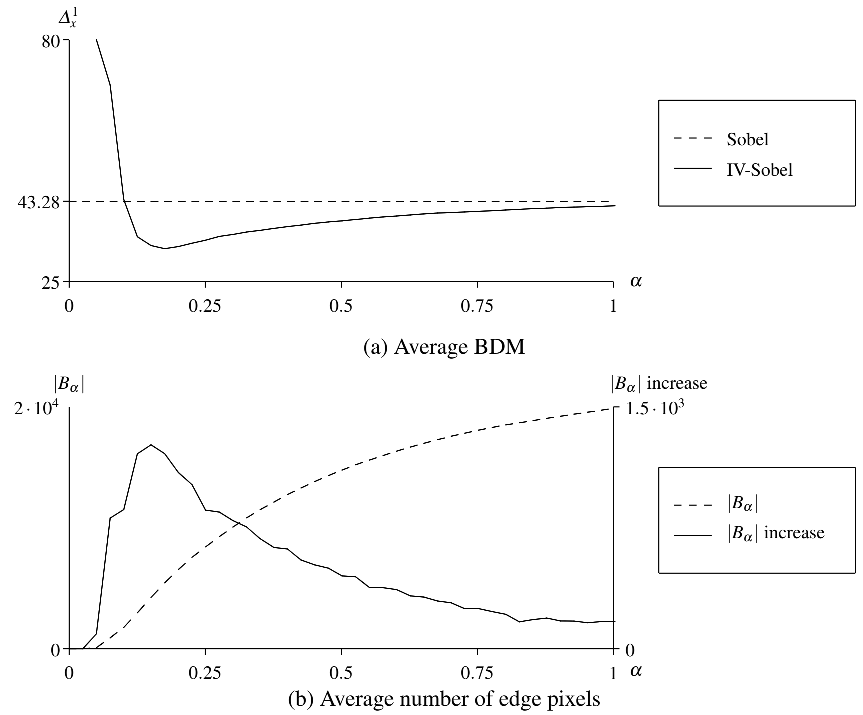

(a) Average BDM

(b) Average number of edge pixels

Fig. 7 Results obtained by the Sobel and IV-Sobel methods on the BSDS test set

In order to confirm these facts, we have repeated the same experiment on the *train* dataset (Fig. 8). Again, we obtain similar results both for the performance (Δ) and the increase of $|B_\alpha|$.

Hence, we can conclude that a proper way to determine α is by experimentally testing a set of them, then selecting the one producing the largest increment of $|B_\alpha|$. The IV-Sobel method is as included in Algorithm 2. Obviously, in this way the first $\alpha = 0$ will never be selected, since its result cannot be compared with any previous B_α.

5 Conclusions

We have analyzed the role of the measurement error in digital images, proposing an interval-valued representation of the image to overcome it. Then, we have proposed a generalization of the Sobel method for edge detection applied on interval-valued images, displaying an example of its use and comparing its performance to the classical Sobel method. We have shown how the performance of the Sobel method can be improved by using the IV representation for ambiguity modeling.

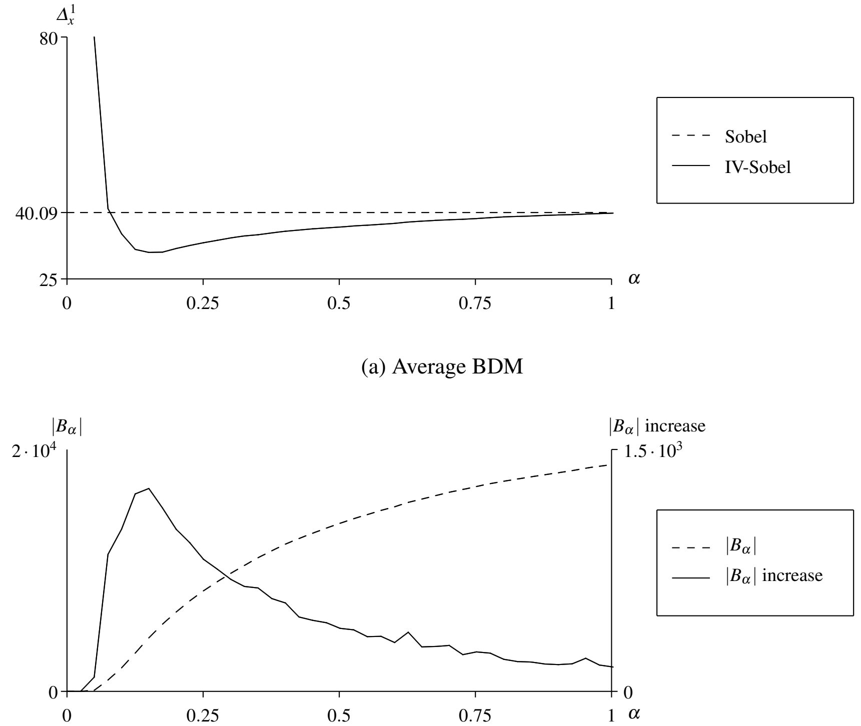

(a) Average BDM

(b) Average number of edge pixels

Fig. 8 Results obtained by the Sobel and IV-Sobel methods on the BSDS train set

```
Data: An image $I$, a optimism indicator step $\delta\alpha$
Result: A binary edge image $B$
begin
    Smoothen $I$ with a Gaussian mask with standard deviation $\sigma_1 = 1.0$;
    Create the IV version of the image, $I_w$;
    Calculate the IV gradient estimations $H_w$ and $V_w$;
    Using the technique in Fig. 4, generate the IV fuzzy edges $E_w$;
    Calculate the candidate $\alpha$, $A \leftarrow \{0, \delta\alpha, 2 \cdot \delta\alpha, \ldots, 1\}$;
    foreach $\alpha \in A$ do
        Create the fuzzy edges as $E_\alpha = K_\alpha(E_w)$;
        Obtain a thin version of fuzzy edge image ($T_\alpha$) using NMS [13];
        Obtain a binary edge image $B_\alpha$ from $T_\alpha$ using Rosin method [14];
    end
    $B \leftarrow$ The $B_\alpha$ producing a larger increment of $|B_\alpha|$;
end
```

Algorithm 2: Final algorithm of the IV-Sobel method with unsupervised selection of the value α.

References

1. F. Jacquey, F. Comby, and O. Strauss. Fuzzy edge detection for omnidirectional images. *Fuzzy Sets and Systems*, 159(15):1991–2010, 2008.
2. S. K. Pal and R. A. King. On edge detection of x-ray images using fuzzy sets. *IEEE Trans. on Pattern Analysis and Machine Intelligence*, 5(1):69–77, 1983.
3. T. Law, H. Itoh, and H. Seki. Image filtering, edge detection, and edge tracing using fuzzy reasoning. *IEEE Trans. on Pattern Analysis and Machine Intelligence*, 18(5):481–491, 1996.
4. L. Hu, H.D. Cheng, and M. Zhang. A high performance edge detector based on fuzzy inference rules. *Information Sciences*, 177(21):4768–4784, 2007.
5. F. Russo. Edge detection in noisy images using fuzzy reasoning. In *Proceedings of the Instrumentation and Measurement Technology Conference*, volume 1, pages 369–372, 1998.
6. J.-A. Jiang, C.-L. Chuang, Y.-L. Lu, and C.-S. Fahn. Mathematical-morphology-based edge detectors for detection of thin edges in low-contrast regions. *IET Image Processing*, 1(3):269–277, 2007.
7. S. Morillas, V. Gregori, and A. Hervas. Fuzzy peer groups for reducing mixed Gaussian-impulse noise from color images. *IEEE Trans. on Image Processing*, 18(7):1452–1466, 2009.
8. I. Sobel and G. Feldman. A 3x3 isotropic gradient operator for image processing. Presented at a talk at the Stanford Artificial Intelligence Project, 1968.
9. M. Galar, J. Fernandez, G. Beliakov, and H. Bustince. Interval-valued fuzzy sets applied to stereo matching of color images. *IEEE Trans. on Image Processing*, 20(7):1949–1961, 2011.
10. J. Canny. Finding edges and lines in images. Technical report, Massachussets Institute of Technology, Cambridge, MA, USA, 1983.
11. V. Torre and T. Poggio. On edge detection. *IEEE Trans. on Pattern Analysis and Machine Intelligence*, 8:147–163, 1984.
12. C. Lopez-Molina, J. Fernandez, A. Jurio, M. Galar, M. Pagola, and B. De Baets. On the use of quasi-arithmetic means for the generation of edge detection blending functions. In *Proceedings of the IEEE International Conference on Fuzzy Systems*, 2010.
13. J. Canny. A computational approach to edge detection. *IEEE Trans. on Pattern Analysis and Machine Intelligence*, 8(6):679–698, 1986.
14. P. L. Rosin. Unimodal thresholding. *Pattern Recognition*, 34(11):2083–2096, 2001.
15. J. M. S. Prewitt. *Object enhancement and extraction*, pages 75–149. Picture Processing and Psychopictorics. Academic Press, 1970.
16. M. Basu. Gaussian-based edge-detection methods- A survey. *IEEE Trans. on Systems, Man, and Cybernetics, Part C: Applications and Reviews*, 32(3):252–260, 2002.
17. G. Papari and N. Petkov. Edge and line oriented contour detection: State of the art. *Image and Vision Computing*, 29(2-3):79–103, 2011.
18. D. Marr and E. Hildreth. Theory of edge detection. *Proceedings of the Royal Society of London*, 207(1167):187–217, 1980.
19. R. Moore. *Interval Analysis*. Prentince-Hall, 1996.
20. D. Martin, C. Fowlkes, D. Tal, and J. Malik. A database of human segmented natural images and its application to evaluating segmentation algorithms and measuring ecological statistics. In *Proceedings of the 8th International Conference on Computer Vision*, volume 2, pages 416–423, 2001.
21. A. J. Baddeley. Errors in binary images and an L^p version of the Hausdorff metric. *Nieuw Archief voor Wiskunde*, 10:157–183, 1992.
22. C. Lopez-Molina, H. Bustince, J. Fernandez, P. Couto, and B. De Baets. A gravitational approach to edge detection based on triangular norms. *Pattern Recognition*, 43(11):3730–3741, 2010.
23. R. Medina-Carnicer, F.J. Madrid-Cuevas, A. Carmona-Poyato, and R. Muñoz-Salinas. On candidates selection for hysteresis thresholds in edge detection. *Pattern Recognition*, 42(7):1284–1296, 2009.
24. J. Weickert, B.M. ter Haar Romeny, and M.A. Viergever. Efficient and reliable schemes for nonlinear diffusion filtering. *IEEE Trans. on Image Processing*, 7(3):398–410, 1998.